Fabrication of a Large-Area Al-Doped ZnO Nanowire Array Photosensor with Enhanced Photoresponse by Straining

Ruey-Chi Wang, Hsin-Ying Lin, Chao-Hung Wang, and Chuan-Pu Liu**

The photosensing properties of flexible large-area nanowire (NW)-based photosensors are enhanced via in situ Al doping and substrate straining. A method for efficiently making nanodevices incorporating laterally doped NWs is developed and the strain-dependent photoresponse is investigated. Photosensors are fabricated by directly growing horizontal single-crystalline Al-doped ZnO NW arrays across Au microelectrodes patterned on a flexible SiO_2/steel substrate to enhance the transportation of carriers and the junction between NWs and electrodes. The Raman spectrum of the Al:ZnO NWs, which have an average diameter and maximum length of around 40 nm and 6.8 μm, respectively, shows an Al-related peak at 651 cm^{-1}. The device shows excellent photosensing properties with a high ultraviolet/visible rejection ratio, as well as extremely high maximum photoresponsivity and sensitivity at a low bias. Increasing the tensile strain from 0 to 5.6% linearly enhances the photoresponsivity from 1.7 to 3.8 AW^{-1} at a bias of 1 V, which is attributed to a decrease in the Schottky barrier height resulting from a piezo-photonic effect. The high-performance flexible NW device presented here has applications in coupling measurements of light and strain in a flexible photoelectronic nanodevice and can aid in the development of better flexible and integrated photoelectronic systems.

1. Introduction

Nanodevices that incorporate nanowires (NWs) have been applied to large areas to enhance the signal-to-noise ratio (S/N) and allow flexible optoelectronics. Therefore, it is desirable to develop large-area NW-based flexible devices and study their strain-dependent properties. 1D nanomaterials, such as ZnO nanorods, have been synthesized on flexible substrates for flexible devices, such as solar cells,[1,2] field-emitting devices,[3,4] light-emitting diodes,[5] and gas sensors.[6] However, these 1D nanomaterials were mostly grown vertically or randomly oriented on substrates, and they were rarely doped with impurities. For fabricating NW-integrated electronic devices, horizontally-aligned and doped 1D nanomaterial arrays in parallel to a substrate are beneficial to carrier transportation and modification of optoelectronic properties in integrated planar devices.

Hydrothermal routes have been used for the low-temperature synthesis of horizontal ZnO 1D NWs on side-active ZnO electrodes.[7,8] However, the obtained NWs are generally low-aspect-ratio, undoped, and short (sub-micrometer). Using a hydrothermal route, Liu et al. developed a ZnO rod flexible strain sensor,[9] whose high sensitivity was mainly attributed to the short ZnO nanorods, enabling the control of the contact area between two sets of ZnO nanorods growing horizontally from the edges of two electrodes by deformation. A contact printing method was used to develop ZnO horizontal NW ultraviolet (UV) sensors on rigid and flexible substrates,[10] but the contacts between the NWs and electrodes were made by pressing a substrate with electrodes onto a horizontal ZnO NW layer on another substrate, and only strain-free photoresponse measurements were taken. The strain-dependent photoresponse of large-area NW photosensors has yet to be investigated.

A prerequisite for achieving reliable strain-dependent photosensing is to ensure sufficiently strong bonding and good junctions between electrodes and NWs, which is difficult to achieve with soft-contact methods such as contact printing. In this paper, a method for efficiently doping laterally grown NWs in nanodevices is developed and used to obtain excellent flexible large-area Al-doped ZnO NW array photosensors, whose strain-dependent photoresponse is investigated. The photosensors were fabricated by directly growing Al-doped ZnO NW arrays horizontally between patterned Au electrodes on flexible SiO_2/steel substrates via modified chemical vapor deposition (CVD), named alloying evaporation deposition,[11] at 650 °C. The doping

Prof. R.-C. Wang
Department of Chemical and Materials Engineering
National University of Kaohsiung
Kaohsiung 81148, Taiwan
E-mail: rcwang@nuk.edu.tw
H.-Y. Lin, C.-H. Wang, Prof. C.-P. Liu
Department of Materials Science and Engineering
National Cheng Kung University
Tainan 70101, Taiwan
E-mail: cpliu@mail. ncku.edu.tw
Prof. C.-P. Liu
Center for Micro/Nano Science and Technology
National Cheng Kung University
Tainan 70101, Taiwan
Research Center for Energy Technology and Strategy
National Cheng Kung University
Tainan 70101, Taiwan
Advanced Optoelectronic Technology Center
National Cheng Kung University
Tainan 70101, Taiwan

DOI: 10.1002/adfm.201200344

of ZnO NWs with Al improves the performance of flexible UV photosensors. This growth scheme can be easily generalized to any optoelectronic nanodevice. The photoresponse measurements of the flexible NW device show a visible-blind UV sensing characteristic with an ultrahigh UV-to-visible rejection ratio of 4.1×10^5 at a low bias of 1 V. In addition, the nanosensor has an ultrahigh photoresponsivity of 3.8 AW^{-1} at 2 V, and excellent sensitivity of above six orders of magnitude at 0.1 V. Bending further enhances the photoresponsivity of the flexible photosensors. This work thus aids the development of high-performance flexible integrated photoelectronic nanodevices to realize strain-dependent photoresponse of large-area nano-photosensors.

2. Results And Discussion

Figure 1a shows a scanning electron microscopy (SEM) image of the layout of the Al:ZnO NW device. Figure 1b–d show low- to high-magnification SEM images of the bridging Al:ZnO NWs. As shown in Figure 1b, NWs can be nucleated from the surface and two side facets of the Au microelectrodes; the horizontal NWs that bridge the two electrodes mostly nucleated from these two side facets. The average diameter of the horizontal NWs is around 40 nm, and the maximum length is above 6.8 μm. The NWs can thus connect two neighboring metallic electrodes with a gap of ≈4 to 6.8 μm, as shown in Figure 1c,d. In the scheme of the design rule for growth, Au is not only pre-patterned for the electrodes but also provides preferential nucleation sites for ZnO NWs to be grown via a vapor-liquid-solid (VLS) mechanism.[12] Among other requirements for NWs to bridge two adjacent electrodes in the sensor chips, a sufficiently high length to diameter ratio, allowing them to lean over, is the most important. However, CVD growth through evaporation and condensation processes often leads to the growth of short and stiff ZnO nanorods. The doping of ZnO with Al was found to increase the aspect ratio and hence the flexibility of ZnO NWs under a given set of growth conditions (see Figure S1 in the Supporting Information for details). As a result, the bent ZnO NWs can make contact with adjacent electrodes, appearing as lateral growth. The increase in the aspect ratio of ZnO NWs may be ascribed to the increased surface energy ratio of (0002) to $(10\bar{1}0)$ of ZnO due to the incorporation of Al dopant, which increases the growth rate ratio of the *c* axis to the *a* axis of wurtzite ZnO NWs. The growth of horizontal NWs benefits electrical contacts and carrier transport in the fabrication of large-area devices. Moreover, the design offers the highest effective surface area for maximum UV light absorption, hence enhancing the performance of the device. Figure 1e shows the energy dispersive X-ray spectroscopy (EDS) spectrum of the NWs, which exhibits strong peaks of Zn and O, and a weak signal of Al. Figure 1f shows the Raman spectrum of the Al:ZnO NWs. The shift of the E_2 vibrational mode from 442 to 437 cm^{-1} indicates the presence of stress resulting from Al doping. In addition, the peak at 651cm^{-1}, assigned to the lattice defects generated by Al doping,[13] confirms the Al doping.

The microstructure of the as-synthesized NWs was characterized by high-resolution transmission electron microscopy (HRTEM). **Figure 2**a shows the TEM bright-field image of an Al-doped ZnO NW. The NW exhibits a straight morphology with sharp edges. Figure 2b,c show the corresponding electron diffraction pattern and high-resolution image, respectively, which reveal that the NW is a single-crystalline wurtzite structure growing along the *c*-axis direction without any visible line or plane defects.

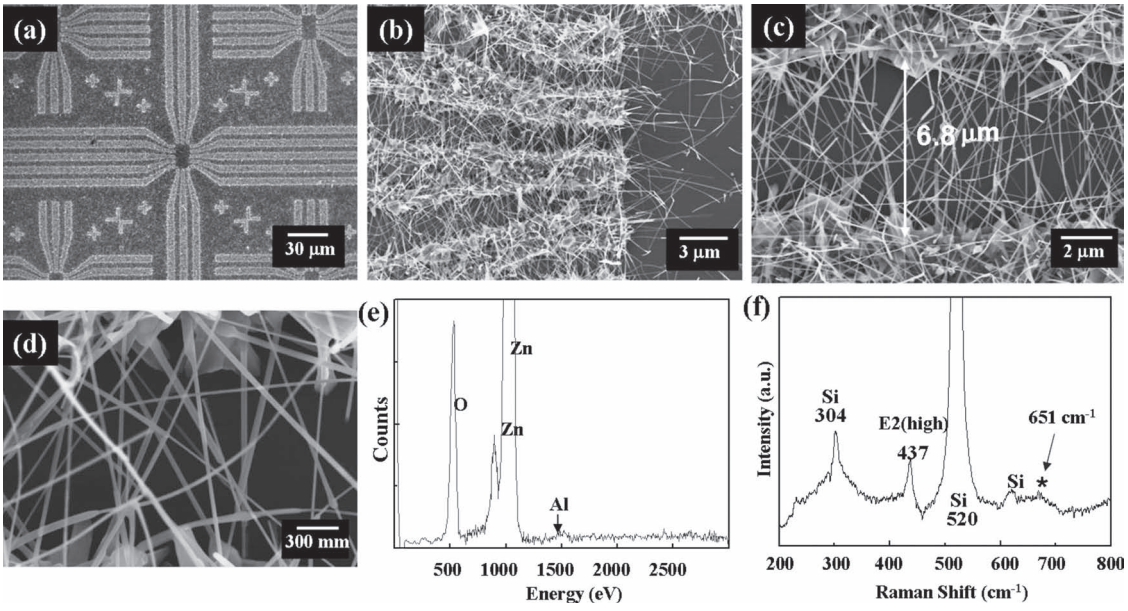

Figure 1. SEM images of a) a whole Al:ZnO NW photosensor, b) NWs bridging the gaps between Au micro-electrodes, and c,d) horizontal NWs. e) EDS and f) Raman spectra of Al:ZnO bridging NWs.

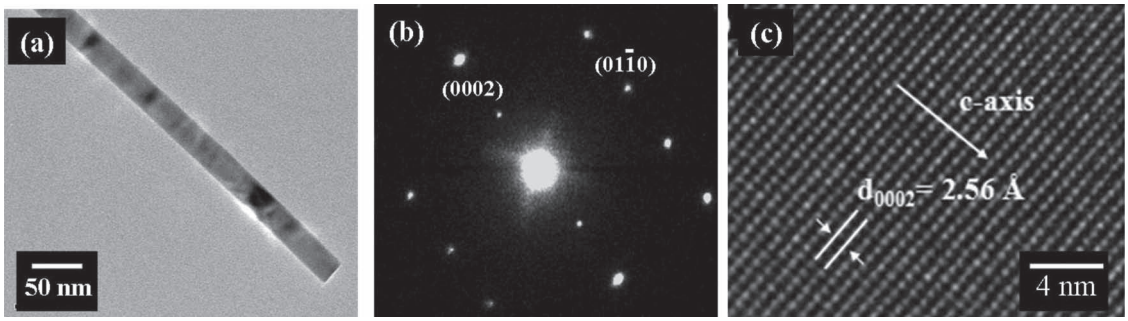

Figure 2. TEM: a) low-magnification bright-field image, b) electron diffraction pattern, and c) high-resolution image of bridging Al:ZnO NWs.

The electrical characteristics and photoresponse of a typical Al: ZnO NW photosensor under various biases are shown in **Figure 3**. Within the chip, electrodes are connected to millimeter-sized pads large enough for an Au-coated steel stylus with micro-tips to make contact with. Only the nearest two electrodes were picked for the photoresponse measurements (see Figure S2 in the Supporting Information). The *I*–*V* curves of the device under dark and UV illumination conditions shown in Figure 3a exhibit a slightly nonlinear characteristic, indicative of a small Schottky barrier present at the contacts between ZnO NWs and Au electrodes. Notably, the dark current is in the range of 10^{-10} A, which is very low and enhances the sensitivity of the sensor. The ultra-low dark current is attributed to the high aspect ratio and optimized structure of the NWs. The dynamic responses of the NW device under UV illumination with a low power density of 60 μW cm^{-2} at biases from 0.1 to 1 V are shown in Figure 3b. When the emission is on, the current of the ZnO NWs initially increases rapidly, and then gradually reaches saturation. Similarly, when the emission is off, the current initially decreases rapidly and then gradually reaches saturation. The first and second response time constants[14] of the device (τ_1 and τ_2) are about 0.1 and 20 s, respectively. The initial fast response is attributed to the photoexcited carrier generation, and the slow response at the second stage is mainly ascribed to photodesorption of the chemisorbed oxygen ions and water molecules on the surface of the ZnO.[15] Photoresponsivity can be calculated from Figure 3b. The results for various biases are shown in Figure 3c. The photoresponsivity increases linearly from 0.2 to 3.8 AW^{-1} as the bias is increased from 0.1 to 2 V. Figure 3d shows the dependence of sensitivity, defined as the ratio of photocurrent to dark current, on applied bias. In contrast to the photoresponsivity, the sensitivity exhibits a non-linear decrease from above six orders of magnitude to five orders of magnitude as the applied bias is increased from 0.1 to 0.4 V, and becomes constant up to 2 V. The photoresponsivity is mainly contributed by the photocurrent, whereas the sensitivity is dominated by the dark current. The dark current shows that an external bias of about 0.35 eV is required to overcome the Schottky barrier height; approximately 0.1 eV is required for under light illumination conditions (see Supporting Information Figure S3a,b for details), apparently due to the generation of photoexcited carriers. The barrier height of 0.35 eV accounts for the ultrahigh sensitivity at low bias.

Considering that the measurements were performed at room temperature, thermionic emission may be the dominant carrier transport mechanism through the barrier. When a relatively large positive voltage is applied across the drain and source, the voltage drop occurs mainly at the reversely biased Schottky barrier φ_s at the source side. Therefore, the current through the Schottky barrier will follow the classic thermionic emission-diffusion theory (for $V >> 3$ kT/q (≈77 mV)), and ln *I* is proportional to $(V)^{1/4}$.[16] The thermionic current mechanism is confirmed by the linear fitting to the curves of ln *I*–$(V)^{1/4}$ under dark and light conditions, with R^2 values larger than 0.99 (see Supporting Information in Figure S4a). When a strong UV light illuminates the sensor, excess photoexcited electrons replenish the depleted region and largely screen the Schottky barrier between ZnO and Au. Given that the area of the Schottky barrier, effective Richardson constant, and donor impurity density are unchanged under UV illumination, the change in Schottky barrier height $^{\Delta}\varphi_s$ due to light illumination can be derived as:

$$\ln[I(\text{light})/I(\text{dark})] = -\rho\phi_s/kT \quad (1)$$

where *I*(light) and *I*(dark) are the currents measured at fixed biases under light and dark conditions, respectively. The change of Schottky barrier height with bias was calculated using Equation (1). A value of 350 meV was obtained at a very low voltage of 0.1 V, which is consistent with the value derived previously. Although this value is much lower than the theoretically predicted value ($q\varphi_B = \varphi_M$-χ_S = 1.2 V) and slightly lower than the 0.4 eV obtained for metalorganic CVD-synthesized ZnO NWs capped with 400-nm-thick Au,[17] it is higher than the 0.2 eV obtained for aqueous-grown ZnO nanorods on Au electrodes.[18] This discrepancy may partly results from the effects of surface defect states, barrier height inhomogeneities, fermi level pinning in NWs, tunneling, and image force lowering on the conduction process.

The performances of the ZnO NW photosensor here are the best yet reported.[10] For example, at a bias of 1 V, the photosensor shows high photoresponsivity (1.7 AW^{-1}) and excellent sensitivity (five orders of magnitude). As discussed previously, the high photoresponsivity and sensitivity are not only attributed to the design of the horizontal NWs between Au electrodes, which are beneficial to electrical contact and transport, but also to the doping of ZnO with Al, which enhances the UV absorption coefficient through donor-bound excitons with a small Schottky barrier height. Considering the electronic structures of the device, in addition to the Schottky barrier generated between ZnO and Au, there is significant band bending resulting from the electron depletion layers near the surface of

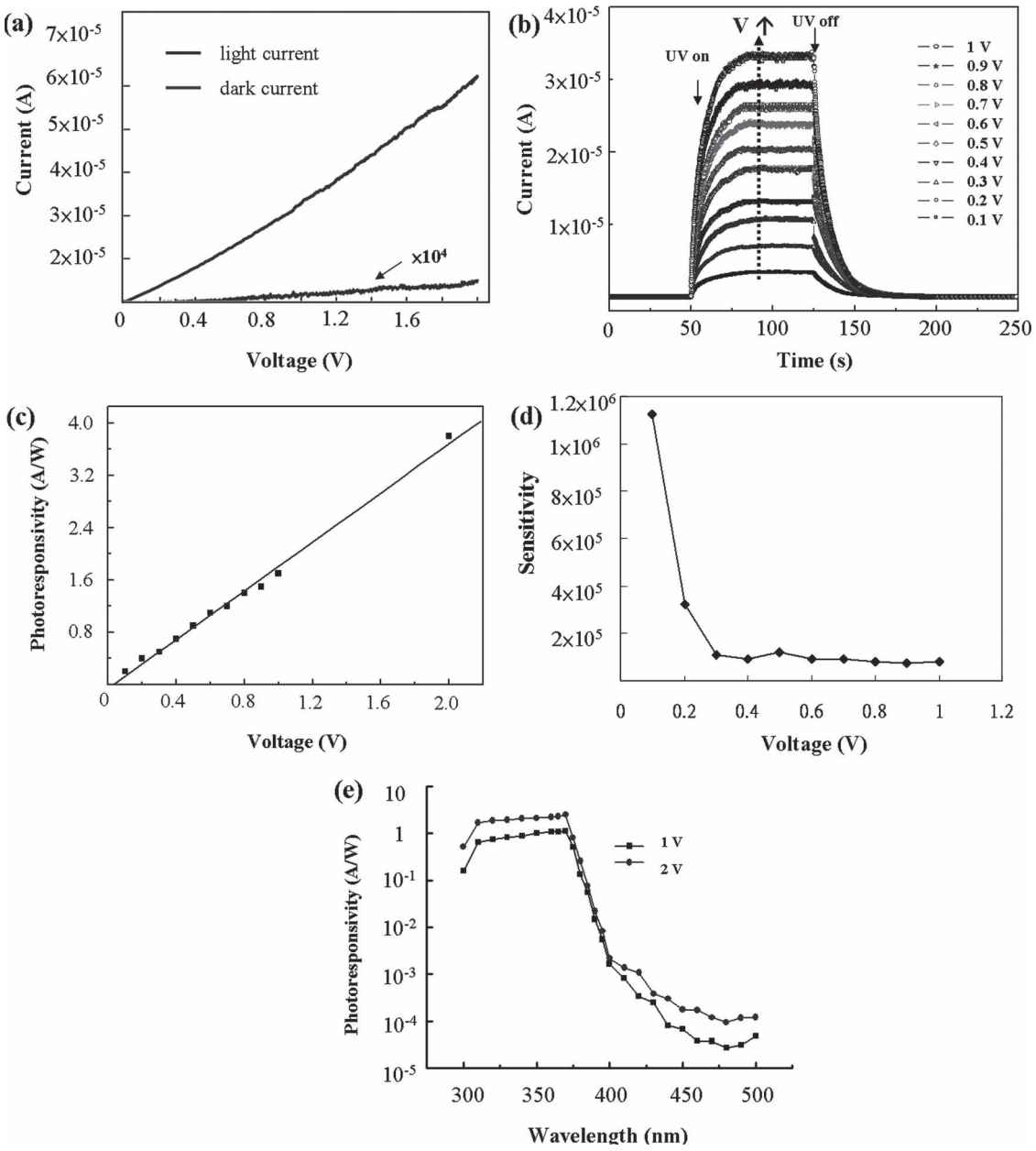

Figure 3. UV photoresponse measurements of an Al:ZnO NW device. a) *I–V* characteristics of the device under dark and UV (centered at 365 nm) illumination. b) Current-time characteristics at various biases under UV illumination with a low power density of 60 μW cm^{-2}. c) Photoresponsivity-voltage relationship. d) Sensitivity-voltage relationship. e) Photoresponsivity spectrum of the device under UV illumination with a low power density of 60 μW cm^{-2} at bias voltages of 1 and 2 V.

the ZnO NW (see Figure S4b in the Supporting Information for details). Therefore, the Schottky barrier height derived above could be partially contributed by interface states induced by Al impurities and larger surface band bending by more absorbed oxygen facilitated by Al dopant at the surface, which in turn contributes more carriers under light excitation through carrier release. According to a previous report,[19] sensitivity increases with Al-doping concentration for concentration of up to 3% in a ZnO gas sensor. Therefore, both sensitivity and photoresponsivity increase with Al doping. Furthermore, Figure 3e shows the spectral response characteristics of the NW photosensor measured at applied biases of 1 V and 2 V. The applied bias does not change the trend. A sharp cutoff appears at 370 nm for the device, corresponding to the energy band gap of ZnO. Notably, the device shows an extremely high UV/visible rejection ratio of 41450, indicative again of an excellent visible-blind UV photosensor.

To further investigate the strain effects on UV sensing properties of Al:ZnO NW arrays, the strain-dependent photocurrent was measured by applying various bending curvatures under

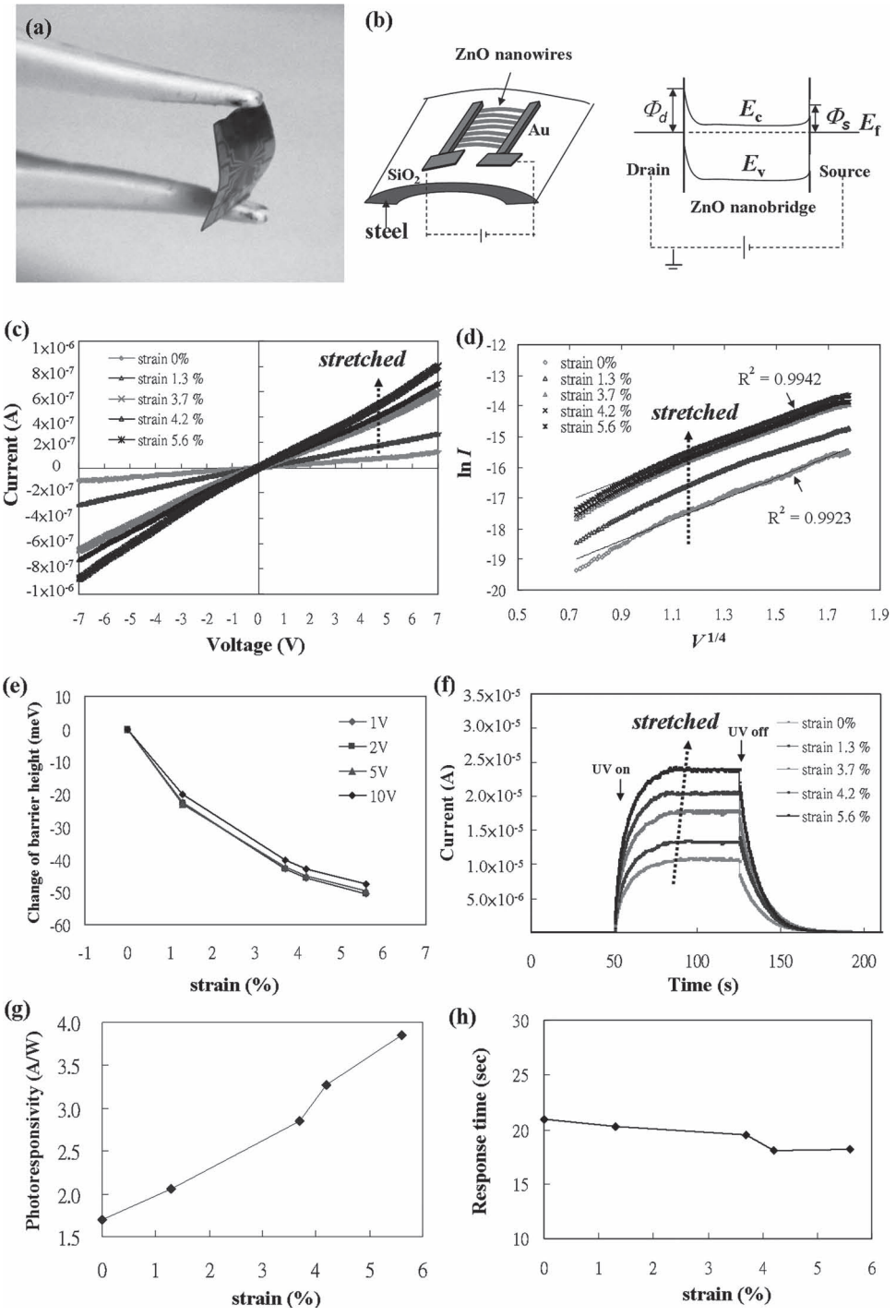

Figure 4. Bending photoresponse measurements of a flexible Al:ZnO NW array chip under UV (365 nm) illumination at a bias voltage of 1 V. a) Photograph of a bent Al:ZnO NW chip. b) Schematic diagram and electronic band diagram of NW device. c) *I–V* characteristics. d) ln *I*-$(V)^{1/4}$ plot. e) Derived change in Schottky barrier height based on the thermionic emission-diffusion model as a function of strain at biases of 1, 2, 5, and 10 V. f) Current-time characteristics at various biases under UV illumination with a low power density of 60 μW cm^{-2}. g) Photoresponsivity-strain relationship. h) Response time-strain relationships of the device under various strains (0 to 5.6%).

UV light illumination. **Figure 4** shows the photosensing measurements of the flexible NW device under bending. The steel substrate withstood a large degree of bending strain, as shown in Figure 4a. When the strains of individual NWs deviates from each other, an averaged strain over all NWs can be represented by the apparent bending strain, which is calculated using the local radius ρ and half thickness of the substrate D as $\varepsilon = +\text{-}D/\rho$[20] (see Figure S5,S6 in the Supporting Information

for details). Individual NWs can be regarded as being subjected to a pure tensile or compressive strain uniformly under such stressing conditions, provided that the size of an NW is much smaller than that of the substrate.[21] A schematic diagram of the bending experiment and electronic band diagram of the device are shown in Figure 4b. Figure 4c shows *I*–*V* curves of the device for various apparent tensile strains (0–5.6%) under illumination by a 365 nm UV laser with a low power of 60 μW cm^{-2}. The *I*–*V* curves show slightly non-linear characteristics, indicative of Schottky contacts, and the photocurrent increases with the apparent strain from 0 to 5.6%. Figure 4d shows the curves of ln *I*–$(V)^{1/4}$ under various strains, which exhibit pretty good linear fitting with R^2 values larger than 0.99. When the curves were fit with other dependencies of *V*, much poorer fittings were obtained. This deviation from an ideal equation of thermionic emission may result from non-uniform characteristics over all the NWs in terms of orientation, contact, and size.

Furthermore, by assuming that the area of the Schottky barrier, effective Richardson constant, and donor impurity density are independent of strain for small deformations, the change in Schottky barrier height $^{\Delta}\varphi_s$ can be derived as:[16]

$$\ln[I(\varepsilon_{zz})/I(0)] = -\rho\phi_s/kT \quad (2)$$

where $I(\varepsilon_{zz})$ and $I(0)$ are the currents measured at a fixed bias with and without applied strain, respectively. Figure 4e shows the calculation results (Equation 1) for biases of 1, 2, 5, and 10 V. The Schottky barrier height decreases with increasing tensile strain, which can result in an increase of current under tensile strain, consistent with the measured results in Figure 4c. Figure 4f shows the dynamic responses of the NW device under various strains at a fixed bias of 1 V. These photocurrents also show a two-step response with first and second response time constants (τ_1 and τ_2) of about 0.1 and 20 s, respectively. Notably, the photoresponsivity varies significantly with strain. Figure 4g shows the relationship between strain and photoresponsivity. The increase in photoresponsivity with tensile strain is ascribed to the increase in current due to a decrease in Schottky barrier height, as shown in Figure 4e. Figure 4h shows the time-strain relationship of the device, indicating that the response time is not significantly changed by the bending of the Al:ZnO NWs. These strain-dependent photoresponse characteristics are based on a combination of band structure change and piezo-phototronic effects coupled with piezo-electric effects, photon excitation, and semiconductor properties.[22]

3. Conclusion

A flexible ZnO-based large-area NW array photosensor was presented. The photosensor was fabricated by depositing Al-doped ZnO NWs to bridge adjacent Au electrodes patterned by standard photolithography procedures on a SiO_2-coated flexible steel substrate. The NWs show a high-aspect-ratio morphology, with an average diameter and maximum length of around 40 nm and 6.8 μm, respectively. The flexible photosensors have excellent photoresponsivity, sensitivity, and UV/visible rejection rate of up to 3.8 AW^{-1}, 1.2×10^6, and 41450, respectively, at a low bias of 0.1 to 2 V. The photoreponsivity is enhanced by the application of a tensile strain on the NWs, which is ascribed to a decrease in the Schottky barrier height for thermionic emission-diffusion transportation. The high-performance large-area flexible NW array photosensor demonstrated here has applications in coupling measurements of light and strain in a flexible integrated photoelectronic system.

4. Experimental Section

An 800-nm-thick SiO_2 film was first deposited on a flexible steel substrate by plasma-enhanced CVD. A bi-layer Ti/Au film with a thickness of 10/100 nm was then deposited onto the flexible SiO_2/steel substrate by electron beam evaporation. Subsequently, the electrode layout was patterned by standard photolithography, as shown in Figure 1a. Horizontal Al-doped ZnO NWs crossing several electrodes were then synthesized on top via alloying evaporation deposition to complete a photosensor device. Zn (purity: 99.8%, 100 mesh) and Al (purity: 99.9%, 100 mesh) mixed powders with a weight ratio of 95:5 were placed in a quartz boat located inside a one-inch-diameter (2.54 cm) horizontal quartz tube reactor. During the growth process, argon was introduced as the carrier gas with a flow rate of 8 sccm, and the working pressure was kept at 50 Torr. The sources were heated at a rate of 20 °C min^{-1} from room temperature to an alloying treatment temperature of 500 °C and held for 30 min to promote the alloying of Al and Zn, which increases the Al vapor pressure from the evaporation of an alloy for Al doping in the growth stage. After the alloying treatment, the total pressure was decreased to 3 Torr and the system was heated at a rate of 20 °C min^{-1} to 650 °C. Then, oxygen was introduced into the chamber with a flow rate of 1 sccm to facilitate the growth of Al:ZnO NWs. After being held at 650 °C for 1 h, the specimen was slowly cooled down to room temperature in the furnace. In the deposition processes, although most of the deposition procedures in this work are similar to those previously reported, the morphology of the as-grown nanostructures significantly varies with even slight changes in deposition parameters, such as working pressure, temperature, source composition, type of substrate, and type of catalyst.

The as-prepared nanostructures were examined by field-emission SEM (4800, Hitachi, Japan) with EDS (XFlash 5030, Bruker, Germany), HRTEM (Tecnai G2 F20, FEI, USA), and Raman spectroscopy (Jobin Yvon LabRAM HR800, France) for morphology, composition, crystallography, and structure characterization, respectively. The electrical and photoresponse measurements were carried out with a Keithley 2400 sourcemeter under UV (365 nm) illumination with a low power density of 60 μWcm^{-2}. The bending experiments of the photosensor device were carried out on a mechanical stage, as schematically shown in Figure S5 in the Supporting Information.

Supporting Information

Supporting Information is available from the Wiley Online Library or from the author.

Acknowledgements

This work was supported by the National Science Council of Taiwan under grants NSC 100-2221-E-390-009-MY3 and NSC 98-2221-E-006-082-MY3.

Received: February 5, 2012
Revised: April 30, 2012
Published online: May 31, 2012

[1] J. Chen, W. Lei, C. Li, Y. Zhang, Y. P. Cui, B. P. Wang, W. Q. Deng, *Phys. Chem. Chem. Phys.* **2011**, *13*, 13182.
[2] J. J. Kim, K. S. Kim, G. Y. Jung, *J. Mater. Chem.* **2011**, *21*, 7730.

[3] J. O. Hwang, D. H. Lee, J. Y. Kim, T. H. Han, B. H. Kim, M. K. Park, K. S. No, S. O. Kim, *J. Mater. Chem.* **2011**, *21*, 3432.
[4] U. N. Maiti, S. Maiti, S. Goswami, D. Sarkar, K. K. Chattopadhyay, *CrystEngComm* **2011**, *13*, 1976.
[5] A. Zainelabdin, S. Zaman, G. Amin, O. Nur, M. Willander, *Nanoscale Res. Lett.* **2010**, *5*, 1442.
[6] J. Yi, J. M. Lee, W. I. Park, *Sens. Actuators B* **2011**, *155*, 264.
[7] S. Xu, Y. Ding, Y. G. Wei, H. Fang, Y. Shen, A. K. Sood, D. L. Polla, Z. L. Wang, *J. Am. Chem. Soc.* **2009**, *131*, 6670.
[8] Y. Qin, R. S. Yang, Z. L. Wang, *J. Phys. Chem. C* **2008**, *112*, 18734.
[9] N. S. Liu, G. J. Fang, W. Zeng, H. Long, L. Y. Yuan, X. Z. Zhao, *J. Phys. Chem. C* **2011**, *115*, 570.
[10] S. Bai, W. W. Wu, Y. Qin, N. Y. Cui, D. J. Bayerl, X. D. Wang, *Adv. Funct. Mater.* **2011**, *21*, 4464.
[11] C. L. Kuo, R. C. Wang, C. P. Liu, J. L. Huang, *Nanotechonology* **2008**, *19*, 035605.
[12] M. H. Huang, Y. Wu, H. Feick, N. Tran, E. Weber, P. Yang, *Adv. Mater.* **2001**, *13*, 113.
[13] S. S. Lo, D. Huang, C. H. Tu, C. H. Hou, C. C. Chen, *J. Phys. D: Appl. Phys.* **2009**, *42*, 095420.
[14] R. Ghosh, D. Basak, *Appl. Phys. Lett.* **2007**, *90*, 243106.
[15] R. C. Wang, C. C. Hsu, S. J. Chen, *Nanotechnology* **2011**, *22*, 035704.
[16] J. Zhou, Y. D. Gu, P. Fei, W. J. Mai, Y. F. Gao, R. S. Yang, G. Bao, Z. L. Wang, *Nano Lett.* **2008**, *8*, 3035.
[17] S. N. Das, J.-H. Choi, J. P. Kar, K.-J. Moon, T. I. Lee, J.-M. Myoung, *Appl. Phys. Lett.* **2010**, *96*, 092111.
[18] K.-I. Ogata, H. Dobashi, P. Russel, K. Koike, S. Sasa, M. Inoue, M. Yano, *Phys. Status Solidi C* **2011**, *8*, 522.
[19] D. Y. Kim, J. Y. Son, *Electrochem. Solid-State Lett.* **2009**, *12*, J109.
[20] R. R. Craig Jr., *Mechanics of Materials*, Wiley, New York **1996**, Ch.6.
[21] J. Zhou, P. Fei, Y. D. Gu, W. J. Mai, Y. F Gao, R. S. Yang, G. Bao, Z. L. Wang, *Nano Lett.* **2008**, *8*, 3973.
[22] X. D. Wang, J. Zhou, J. H. Song, J. Liu, N. S. Xu, Z. L. Wang, *Nano Lett.* **2006**, *6*, 2768.